

## Into thin air: contributions of aerodynamic and inertial-elastic forces to wing bending in the hawkmoth *Manduca sexta*

S. A. Combes\* and T. L. Daniel

Department of Biology, University of Washington, Seattle, WA 98195, USA

\*Author for correspondence (e-mail: scombes@u.washington.edu)

Accepted 18 May 2003

### Summary

During flapping flight, insect wings must withstand not only fluid-dynamic forces, but also inertial-elastic forces generated by the rapid acceleration and deceleration of their own mass. Estimates of overall aerodynamic and inertial forces vary widely, and the relative importance of these forces in determining passive wing deformations remains unknown. If aeroelastic interactions between a wing and the fluid-dynamic forces it generates are minor compared to the effects of wing inertia, models of insect flight that account for passive wing flexibility would be far simpler to develop. We used an experimental approach to examine the contributions of aerodynamic and inertial-elastic forces to wing bending in the hawkmoth *Manduca sexta*. We attached fresh *Manduca* wings to a motor and flapped them at a realistic wing-beat frequency and stroke amplitude. We compared wing bending in normal air versus helium (approx. 15% air density), in which the

contribution of fluid-dynamic forces to wing deformations is significantly reduced. This 85% reduction in air density produced only slight changes in the pattern of *Manduca* wing deformations, suggesting that fluid-dynamic forces have a minimal effect on wing bending. We used a simplified finite element model of a wing to show that the differences observed between wings flapped in air versus helium are most likely due to fluid damping, rather than to aerodynamic forces. This suggests that damped finite element models of insect wings (with no fluid-dynamic forces included) may be able to predict overall patterns of wing deformation prior to calculations of aerodynamic force production, facilitating integrative models of insect flight.

Key words: insect flight, wing flexibility, wing bending, aerodynamic forces, inertial forces, finite element model, *Manduca sexta*.

### Introduction

Flapping wings produce a variety of forces as they accelerate and decelerate through a fluid medium. Some of these forces, such as aerodynamic and added-mass forces, are related to the fluid through which the wing moves, while others, such as inertial-elastic forces, are determined solely by the mass of the wing and its material properties. In insects, these forces bend and twist the wings during flight, resulting in passive shape changes that may affect many aspects of flight performance, from the lift-to-drag ratio of wings (Batchelor, 1967) to thrust production and fluid-dynamic efficiency (Combes and Daniel, 2001; Daniel, 1987; Wu, 1971). Because insect flight muscles are restricted to the wing base, these passive shape changes are controlled primarily by the architecture and material properties of the wing; in many cases, these design features appear to permit certain beneficial deformations (e.g. lift-enhancing torsion; Wootton, 1990), while preventing detrimental bending. Being able to predict large, dynamic shape changes is essential for developing a comprehensive understanding of insect flight, as instantaneous wing shape helps determine the direction and magnitude of fluid-dynamic forces generated by the wing (Batchelor, 1967). If, in turn, these fluid-dynamic forces are important in determining dynamic wing shape, predictions of

wing bending must be coupled in each time step to calculations of the aerodynamic forces generated by these shapes, a difficult and time-consuming task. However, if inertial-elastic (fluid-independent) forces dominate wing bending, the dynamic shape of flapping wings could be predicted prior to calculations of aerodynamic force production, avoiding the coupled aeroelastic problem.

In some insect species, such as *Drosophila*, wing bending is limited, and physical or mathematical models that assume the wings are rigid can provide significant insights into mechanisms of unsteady force production (e.g. Dickinson et al., 1999; Ramamurti and Sandberg, 2002; Sane and Dickinson, 2002; Sun and Tang, 2002a). However, the wings of many species, such as *Manduca*, bend and twist dramatically during flight (Dalton, 1975; Wootton, 1990), particularly during slow flight and hovering (Willmott and Ellington, 1997). Most computational models of flight in *Manduca* have accounted for wing bending by incorporating simplified shape changes that are specified in advance (Liu et al., 1998; Liu and Kawachi, 1998); these approaches have contributed substantially to our understanding of fluid dynamic force generation in specific situations, such as during hovering flight. However, models of insect flight

incorporating passive wing deformations could be used to address further questions of functional wing morphology and evolution, as well as to explore the effects of alternative kinematic patterns on dynamic wing shape and insect flight performance.

Unfortunately, the development of these integrative models has been hindered by uncertainty about the relative importance of fluid-dynamic and inertial-elastic forces in determining dynamic wing shape. Some estimates of overall wing inertia (averaged spatially and/or temporally) suggest that inertial forces are generally higher than aerodynamic forces (Ellington, 1984b; Lehmann and Dickinson, 1997; Wilkin and Williams, 1993; Zanker and Gotz, 1990), whereas other studies conclude the opposite (Sun and Tang, 2002b; Wakeling and Ellington, 1997). A limited number of theoretical studies addressing local bending moments in flapping wings suggest that inertial-elastic forces may play a larger role than aerodynamic forces in determining instantaneous wing shape. For example, Ennos (1989) estimated that spanwise bending moments due to the inertia of flapping wings are at least twice as large as those due to aerodynamic forces, and showed that wing inertia alone could cause the tip-to-base torsional wave seen in many insect wings during supination (Ennos, 1988). Daniel and Combes (2002) showed that chordwise bending moments generated by elastic wave propagation in flapping insect wings (inertial-elastic effects) are significantly larger than the moments exerted on wings by the surrounding fluid.

In this study, we used an experimental approach to examine the relative contributions of inertial-elastic and fluid-dynamic forces to passive wing bending. We attached fresh *Manduca sexta* wings to a motor and flapped them around the dorsal-ventral axis of the wing hinge at a realistic wing-beat frequency and stroke amplitude, mimicking the large-amplitude motions of freely flying moths. We used high-speed video recording to compare instantaneous wing deformations of wings flapped in normal air *versus* helium (approx. 15% air density). The lower density of helium substantially reduces the contribution of fluid-dynamic forces to the observed wing deformations, allowing us to determine the relative importance of these forces in passive wing bending.

At the same time, however, this lower fluid density also reduces external damping of the wing's motions. We used a simplified finite element model based on a *Manduca* wing to explore how damping alone (in the absence of fluid-dynamic forces) affects wing motions. Because the finite element analysis does not include fluid-dynamic forces, the motions of the model wing depend solely on structural features and inertial-elastic effects. We subjected the model to the same motions as real wings, and compared bending patterns in the undamped model wing to those of the model with damping added.

## Materials and methods

### Dynamic bending experiments

We anaesthetized hawkmoths *Manduca sexta* (Linnaeus 1763) from a colony at the University of Washington at 0°C

for 5 min, then removed one forewing at the base and recorded wing mass. We did not include the smaller, overlapping hindwings in this study, as their position relative to the forewings is variable during flight, and this interaction is difficult to recreate when the wings are detached from the animal. We marked three spots on the forewing with a small dot of reflective white paint (weighing  $\leq 1.5\%$  of total wing mass) on both the dorsal and ventral sides: the wing tip, the trailing edge (where chord length is maximum, approximately 50% wing span), and the leading edge (at the same spanwise position; Fig. 1A). We used cyanoacrylate glue cured with baking soda to attach the base of the wing to a brass rod that could be rotated by an oscillator constructed from the pen motor and amplifier of a Gould chart recorder (Fig. 1A).

The motor was attached to a platform inside a 30 cm Plexiglass box (with 1 cm thick walls) and its motion was

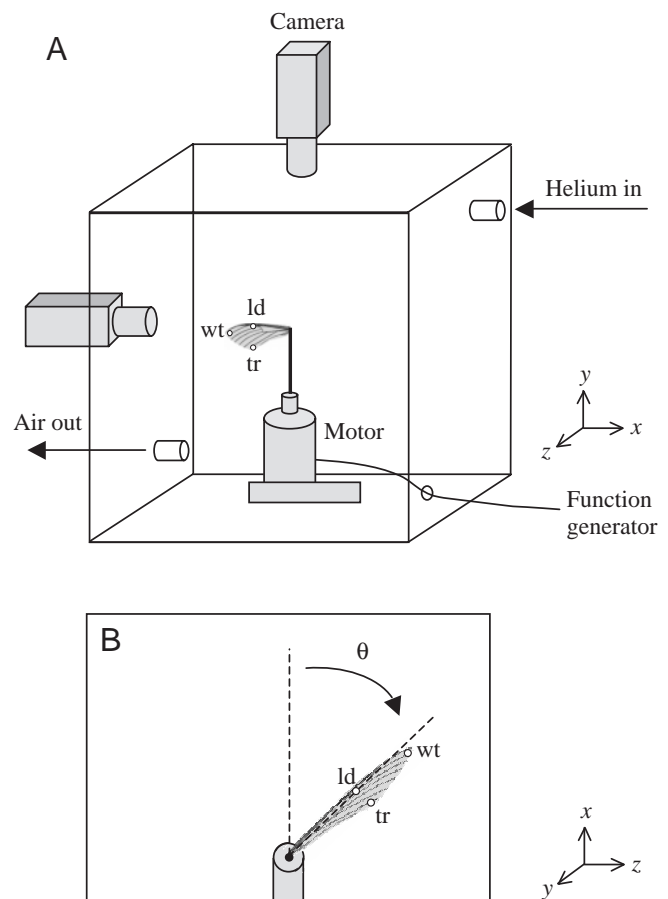


Fig. 1. Apparatus used to visualize *Manduca sexta* wing bending in normal air and helium. (A) Each wing was marked with dots of reflective paint at the wing tip (wt), leading edge (ld) and trailing edge (tr) and filmed from orthogonal views while flapping around the dorsal-ventral axis of the wing hinge (the y-axis). After filming, air was repeatedly removed from the box and replaced with helium until the box was filled with >95% helium. Wings were then filmed while flapping at the same amplitude and frequency. (B) Coordinates of the marked points were digitized and converted into angular position ( $\theta$ ), with the origin at the wing base and position (viewed from the leading edge) measured from the center of rotation.

controlled with a function generator. Wings were flapped sinusoidally around the dorsal–ventral axis of the wing hinge at room temperature. Total amplitude varied between  $107^\circ$  and  $110^\circ$ , corresponding to intermediate stroke amplitudes in free-flying hawkmoths (Willmott and Ellington, 1997). Wing motions were recorded by two high-speed video cameras (Redlake Inc., San Diego, CA, USA) at  $1000 \text{ frames s}^{-1}$ , one viewing the wing from its leading edge and the other from its tip (Fig. 1A).

Each wing was filmed while flapping at 0.5 Hz, as a control for the shape and position of the wing when no dynamic bending occurs, and at 26 Hz, a typical wing-beat frequency for *Manduca sexta* (Willmott and Ellington, 1997). The density of fluid inside the chamber was then reduced by repeatedly removing air through an opening near the bottom of the box and adding helium through an opening near the top (Fig. 1A). The wing was filmed flapping at 26 Hz in a mixture of no less than 95% helium, which has a density of  $0.164 \text{ g l}^{-1}$  (approximately 14% of normal air density; CRC, 2001). Finally, the box was opened to release the helium and the wing was again filmed at 26 Hz in normal air, to check for potential wing damage. All filming was completed within 1 h, during which time the flexural stiffness of the wing does not change appreciably (Combes, 2002). The procedure was repeated on four different wings from three individuals.

#### Wing bending analysis

We analyzed frames from three complete flaps in the middle of each filming sequence, to avoid bending artefacts at the onset of motion. A custom Matlab program (developed by M. S. Tu) identified the coordinates of the wing tip, leading edge and trailing edge in each frame. These three-dimensional Cartesian coordinates were converted to spherical coordinates, using the wing base as the origin and measuring the position of the wing (viewed from the leading edge) in degrees, with  $0^\circ$  at the center of rotation (Fig. 1B). Flapping frequency was found by dividing the number of complete flaps by the total number of frames and multiplying by 1000. Amplitude applied by the motor was measured at the leading edge in the control sequence (0.5 Hz) to avoid wing bending, using the maximum excursion of the leading edge marker to define the sides of a right triangle. To determine if amplitude applied at the base changes significantly with flapping frequency, a brass rod of the same length and mass as a *Manduca* wing was attached to the motor and filmed at 0.5 Hz and 26 Hz.

To examine temporal patterns of bending at each wing location, we compared the trajectory of a wing flapping at 26 Hz and at 0.5 Hz (where no dynamic bending occurs), adjusting the time base of the control sequence to match that of the experimental sequence and splining data to equal time intervals in Matlab. We then calculated the difference in position at each time point and performed a Fourier analysis on this wing bending data to determine the dominant frequencies of wing motion and the amplitude coefficient at each frequency.

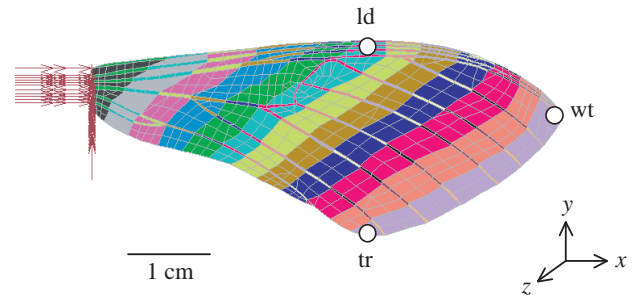


Fig. 2. Finite element model based on a *Manduca sexta* wing. The model approximates the planform geometry, vein configuration and spatial variation in flexural stiffness of a real wing. Declining material stiffness ( $E$ ) of membrane and vein elements results in an exponential decline in flexural stiffness ( $EI$ ), as measured in *Manduca* wings (Combes, 2002; Combes and Daniel, 2003b). Each color represents a different value of material stiffness, which varies from  $4.7 \times 10^7 \text{ N m}^{-2}$  to  $4.5 \times 10^9 \text{ N m}^{-2}$  in membrane elements, and from  $1.9 \times 10^{11} \text{ N m}^{-2}$  to  $1.8 \times 10^{13} \text{ N m}^{-2}$  in vein elements. The wing was rotated at its base around the  $y$ -axis, and bending was analyzed by tracking the positions of nodes at the wing tip (wt), leading edge (ld) and trailing edge (tr).

#### Finite element modeling

As a wing is flapped through the air and deformed by inertial and/or aerodynamic forces, its motions are damped by some combination of internal (e.g. elastic or structural) and external (fluid) mechanisms. When the surrounding fluid is less dense (as is the case with the *Manduca* wings flapped in helium) the wing experiences less external damping. We explored how damping affects wing bending by constructing a simplified finite element model (FEM) based on a male *Manduca* forewing, and comparing bending in the undamped wing to bending in the model wing with damping added. The model was created in MSC Marc/Mentat and is composed of thin shell elements of uniform thickness, recreating the planform configuration of veins and membranes in a real wing (but omitting details of three-dimensional wing structure; see Combes and Daniel, 2003b). We applied declining values of material stiffness to the model wing in 12 strips, oriented diagonally (Fig. 2); these strips are perpendicular to most of the wing veins, which decrease in diameter towards the wing edge and thus are likely to decrease in stiffness along this axis. This configuration results in an exponential decline in flexural stiffness  $EI$  (the product of Young's modulus  $E$  and the second moment of area  $I$ ) in both the spanwise and chordwise directions of the wing, approximating patterns of flexural stiffness measured in real wings (Combes, 2002; Combes and Daniel, 2003b). Within each strip, vein elements have a higher material stiffness than membrane elements, mimicking the increased flexural stiffness of tubular veins. We used an element density of  $1200 \text{ kg m}^{-3}$  (as measured in insect wings; Wainwright et al., 1982), a thickness of  $45 \mu\text{m}$ , and a Poisson's ratio of 0.49 (consistent with measured values of biological materials; Wainwright et al., 1982). To determine the minimum number of elements necessary to capture the bending

behavior of wings, we performed a sensitivity analysis with models composed of 200, 350, 865 and 2300 total elements, and found that 865 elements are sufficient to ensure asymptotic performance of the model.

We applied boundary conditions to the nodes at the wing hinge so that they could not translate in any direction and could rotate only along the dorsal–ventral axis, as in experiments on real wings (Fig. 2, red arrows). We began the simulation with

initial conditions of zero displacement and zero velocity at all nodes, and gradually increased the rotation at the wing hinge to a sinusoidal motion with the following function:

$$\theta(t) = (1 - e^{-t/\tau})\sin(\omega t), \quad (1)$$

where  $\theta$  is rotation at the base nodes,  $t$  is time in s,  $\tau$  is the time constant and  $\omega$  is the angular frequency ( $2\pi f$ , where  $f$  is the flapping frequency). We flapped the wing at 26 Hz, and found

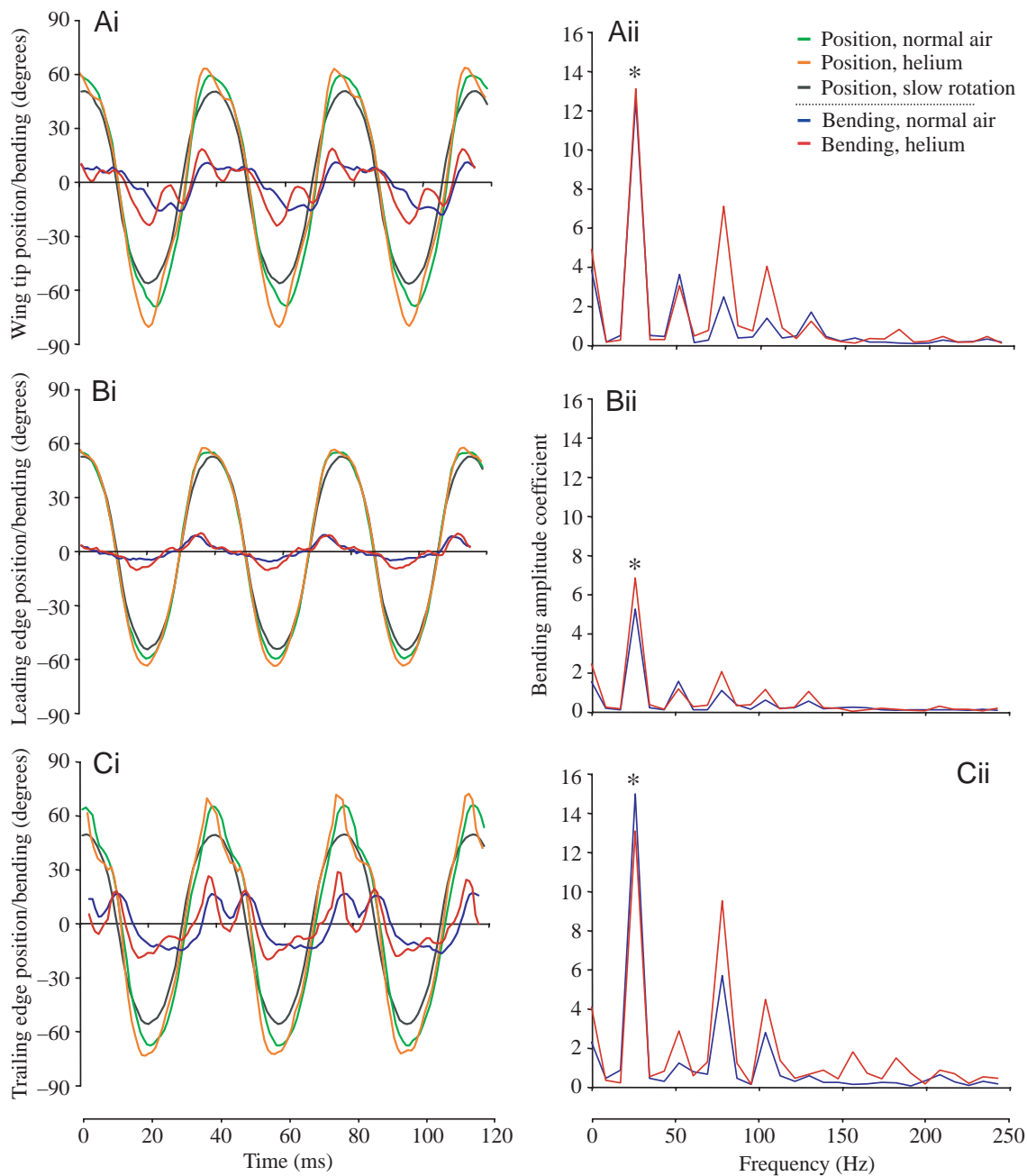


Fig. 3. (Ai–Ci) Angular position and bending at the wing tip (A), leading edge (B) and trailing edge (C) of a *Manduca* wing flapped in normal air *versus* helium. The time base of 0.5 Hz control sequences (slow rotation) was adjusted to match 26 Hz experiments for comparison. At each of the wing locations, angular position during the control sequence (slow rotation; black line) was subtracted from position during the 26 Hz sequences in normal air or helium (green or orange lines) to quantify temporal patterns of wing bending (blue or red lines). (Aii–Cii) Amplitude coefficients from Fourier analyses of wing bending in normal air and helium are shown on the right, with the driving frequency of 26 Hz indicated by asterisks.

that a time constant ( $\tau$ ) of 1/20 s avoids transient artefacts of rapid initial acceleration and allows the wing to reach its full stroke amplitude of  $108^\circ$  (the mean amplitude of experiments on real wings) after 6.5 flaps.

We performed one simulation with no damping added to the computational analysis, and another in which we added mass damping, adjusting the level of damping to best represent the observed changes in motion between real wings flapped in normal air *versus* helium. We ran each simulation for 19200 time steps, recreating 12.5 flaps in 0.48 s, and measured displacement of nodes at the wing tip, leading edge and trailing edge (in the same locations as on real wings; Fig. 2), through six flaps after the wing motion had reached full amplitude. To provide a control with no dynamic bending (analogous to the slow rotation in the experiments), we created a stiff wing by changing the Young's modulus of all elements to  $1 \times 10^{16} \text{ N m}^{-2}$ , and subjected this wing to the same motions as the flexible wings. We quantified temporal patterns of wing bending at each of the wing locations by finding the difference in position between the stiff wing and the flexible wing (with and without damping), and performed a Fourier analysis on the resulting data.

## Results

### Wing bending experiments

The frequency at which *Manduca* wings were flapped varied from 25.5 to 26.9 Hz ( $\bar{x}=26.2$  Hz) in experimental sequences, and from 0.56 to 0.57 Hz ( $\bar{x}=0.565$ ) in control sequences. Flapping amplitude during control sequences varied from  $107.1^\circ$  to  $109.9^\circ$  ( $\bar{x}=108.0^\circ$ ). Amplitude of the brass rod changed by only 1.7% when flapped at 0.57 Hz and 26.3 Hz, indicating that amplitude applied at the base during

experimental sequences is not significantly different from that applied during control sequences. Wing tip, leading edge and trailing edge trajectories from sequences recorded in normal air at the end of the experiment were indistinguishable from those recorded at the beginning (Combes, 2002), confirming that the experimental procedure does not damage wings. Data from only the initial sequence in normal air were used for further analysis.

In control sequences, the angular positions of the wing tip, leading edge and trailing edge were nearly identical (black lines, Fig. 3) and total amplitude was equivalent to the amplitude applied at the base, demonstrating that no dynamic bending occurs at these low frequencies. When flapping frequency was increased during experimental sequences, peak amplitudes at the wing tip and trailing edge increased, indicating that wings bent considerably at the end of each stroke (Fig. 3Ai–Ci), while amplitude at the leading edge changed only slightly (Fig. 3Bi).

Wings flapped in helium displayed slightly higher peak amplitudes than those flapped in normal air, but patterns of bending were similar (Fig. 3Ai–Ci; see also <http://faculty.washington.edu/danielt/movies> for movies of flapping wings). Fourier analysis reveals that the dominant frequencies of wing bending were the same in both helium and normal air, and that only the amplitude of some higher harmonics differed (Fig. 3Aii–Cii; Table 1). Amplitude coefficients were similar in normal air and helium at the driving frequency (26 Hz), but were often larger in helium at higher harmonics, particularly at the second harmonic (78 Hz; Table 1).

### Finite element modeling

In the stiff FEM wing, the angular positions of the wing tip, leading edge and trailing edge were identical (Fig. 4, black lines) and equivalent to amplitude at the base; thus, as in

Table 1. Amplitude coefficients from Fourier analyses of wing bending at the tip, leading edge and trailing edge of *Manduca* wings

Wing		Amplitude coefficient							
		26 Hz*		52 Hz		78 Hz		104 Hz	
		Normal	Helium	Normal	Helium	Normal	Helium	Normal	Helium
Wing tip	1	12.675	10.641	1.540	<b>3.999</b>	3.747	<b>9.012</b>	1.347	1.190
	2	12.196	10.706	1.289	<b>3.496</b>	3.050	<b>9.083</b>	1.437	<b>3.367</b>
	3	13.235	11.856	2.783	2.744	2.710	<b>10.049</b>	1.514	<b>3.739</b>
	4	12.545	13.097	3.613	3.041	2.465	<b>7.077</b>	1.372	<b>4.025</b>
Leading edge	1	4.620	4.323	0.906	0.798	1.524	2.564	0.119	<b>0.614</b>
	2	3.486	4.452	1.026	0.911	1.126	<b>3.014</b>	0.231	0.436
	3	3.801	5.280	0.901	0.687	0.896	<b>2.906</b>	0.469	0.858
	4	5.236	6.817	1.561	1.175	1.092	2.045	0.595	1.120
Trailing edge	1	11.386	9.904	1.157	<b>2.677</b>	3.626	<b>10.295</b>	1.227	<b>5.581</b>
	2	12.589	9.794	1.341	2.536	4.467	<b>9.553</b>	1.519	<b>4.666</b>
	3	14.034	10.564	0.870	1.629	5.228	<b>10.714</b>	1.377	<b>4.206</b>
	4	14.965	13.062	1.222	<b>2.856</b>	5.680	9.485	2.779	4.470

Coefficients at the driving frequency (26 Hz; asterisk) and first three harmonics are shown for each wing in normal air and in helium. Cases where the coefficient in helium varied by more than 100% from the coefficient in normal air are shown in bold.

control sequences on real wings, the stiff FEM wing displayed no dynamic bending. In the flexible FEM wings, maximum tip and trailing edge amplitudes were higher than the amplitude applied at the base, while the leading edge amplitude changed only slightly (Fig. 4Ai–Ci). Although bending amplitude at the trailing edge of the FEM wings was lower than in real *Manduca* wings, temporal patterns of wing bending were similar (Figs 3Ai–Ci, 4Ai–Ci).

In addition, the differences between the FEM wing with no

damping and the wing with mass damping were similar to those seen between real wings flapped in helium and in normal air. The undamped model wing showed slightly higher peaks in wing bending (Fig. 4Ai–Ci), but the same overall bending pattern as the damped wing. Fourier analysis revealed that the dominant frequencies of bending were the same in the two simulations, and that amplitude coefficients were similar at the driving frequency and larger in the undamped model at higher frequencies (Fig. 4Aii–Cii).

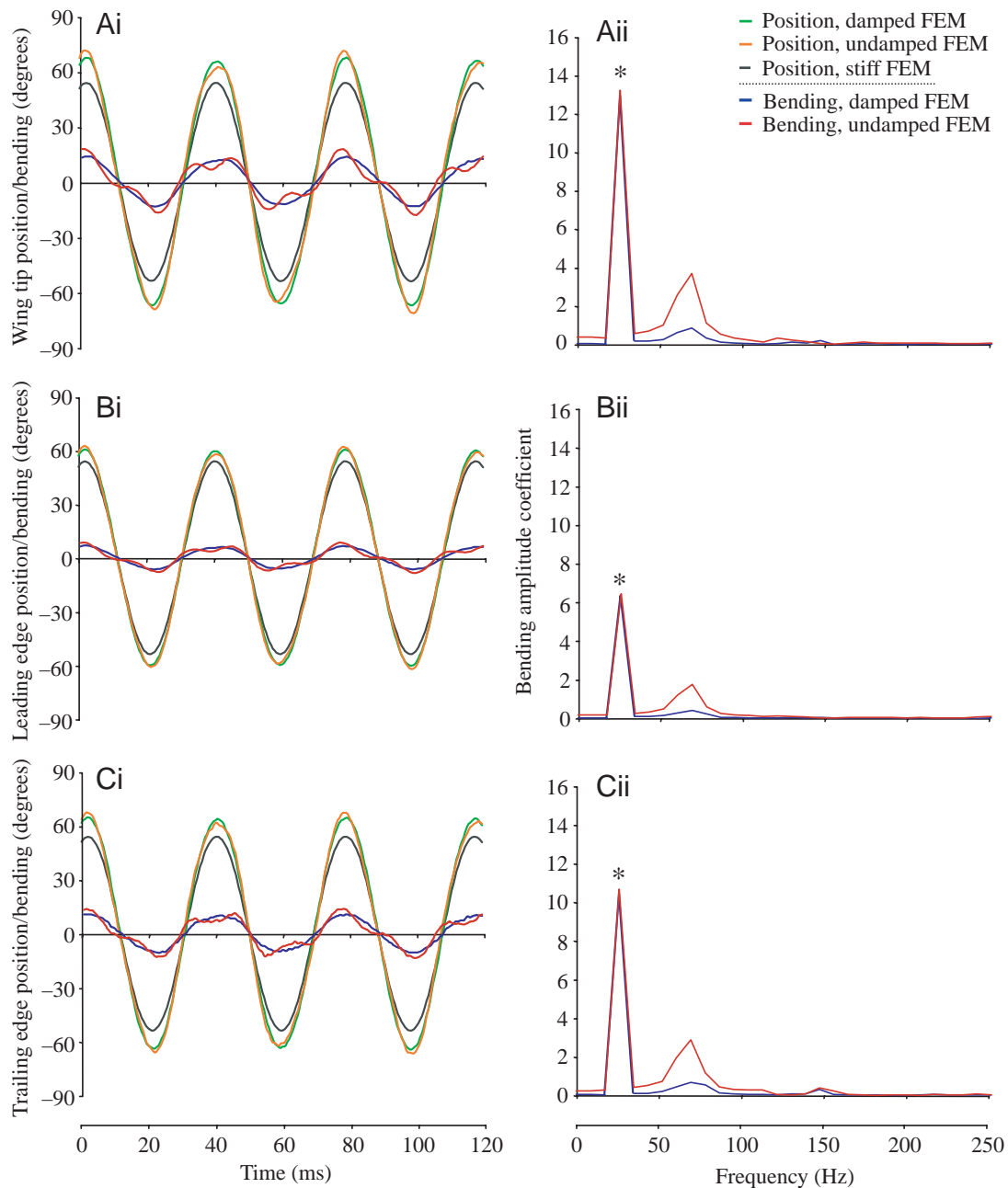


Fig. 4. (Ai–Ci) Angular position and bending at the wing tip (A), leading edge (B) and trailing edge (C) of a finite element model based on a *Manduca* wing. Wing bending was calculated as in Fig. 3, by finding the difference between the angular position of a stiff wing (black line; analogous to the 0.5 Hz control sequence in real wings) and that of a flexible model wing, with or without mass damping (green or orange lines). (Aii–Cii) Amplitude coefficients from Fourier analyses of wing bending in the damped *versus* undamped model are shown on the right, with the driving frequency of 26 Hz indicated by asterisks.

## Discussion

### *Aerodynamic versus inertial-elastic forces in Manduca wing bending*

Our measurements of regional wing bending show that flapping *Manduca* wings undergo significantly more dynamic bending at the wing tip and trailing edge than along the leading edge, confirming previous static measurements of regional flexural stiffness (Combes and Daniel, 2003b). Wings flapped in helium displayed similar spatial and temporal bending patterns and the same dominant frequencies of motion as wings flapped in normal air, despite an 85% reduction in fluid density. This demonstrates that the contribution of aerodynamic loading to instantaneous wing shape in *Manduca* is minor compared to the contribution of wing inertia.

Although overall patterns of bending were remarkably similar, high-frequency components of bending motion were more pronounced in wings flapped in helium (Fig. 3Aii–Cii); this was manifested visually as rapid oscillations in the more flexible regions of the wing, particularly as the wing slowed and began to move in the opposite direction. Simulations of wing bending in the finite element model suggest that reduced damping may explain this difference. Adding damping to the finite element analysis reduced higher-frequency components of motion in the model wing, just as increasing the density of the fluid (by using normal air as opposed to helium) reduced higher-frequency components of motion in real wings (Figs 3Aii–Cii, 4Aii–Cii).

These results suggest that a damped finite element model (with realistic, three-dimensional forces applied at the base) could be successful in predicting the overall pattern and magnitude of *Manduca* wing deformations during flight, independent of aerodynamic calculations. The finite element model used in this study contains several simplifications in three-dimensional geometry that may limit its ability to predict wing motions precisely. In addition, we did not incorporate an accurate distribution of wing mass, which declines sharply towards the tip and trailing edges (although preliminary simulations suggest that mass distribution affects primarily the magnitude, not the pattern of wing bending). Yet even this simplified model was able to simulate temporal and regional wing bending patterns relatively well, suggesting that a slightly more detailed finite element model could provide very accurate results.

To recreate *Manduca* wing motions during flight precisely, the boundary conditions at the base of the model wing would also need to be altered. The experimental work and dynamic modeling in this study were based on a relatively simple kinematic pattern, in which the wing was rotated around only the dorsal–ventral axis of the wing hinge. In most insects, muscular forces transmitted to the wing base not only propel the wing with large amplitude motions such as these, but also rotate the wing around its leading edge, controlling the angle of attack of the wing and, in some cases, causing significant spanwise twisting. The rapid wing rotations evident in some species during stroke reversal (e.g. Dickinson et al., 1999)

may involve increased aerodynamic forces, as well as rapid accelerations and decelerations that could augment inertial-elastic forces. The extent to which more detailed kinematics might alter our findings about the relative contributions of aerodynamic and inertial-elastic forces to wing bending remains a subject of future study.

It is also important to note that the relative contributions of aerodynamic and inertial-elastic forces to wing bending are likely to vary along a continuum, from hovering, where inertial-elastic forces appear to dominate in *Manduca*, to the extreme case of steady, forward flight with no flapping, where inertial forces are negligible and any wing bending would be due solely to aerodynamic forces. In many insects, however, the most pronounced wing bending and twisting occurs during slow flight or hovering (e.g. in *Manduca*; Willmott and Ellington, 1997), so passive deformations may in fact decrease as aerodynamic forces begin to dominate.

### *Insect size and wing design*

Because the *Manduca* wings used in this study are relatively large and heavy, it is possible that inertial-elastic effects are more important in determining wing bending in this species than in other species with smaller, lighter wings. A simple analysis of average bending moments can be used to assess the relative magnitudes of inertial-elastic and aerodynamic moments on the flapping wings of different species (Daniel and Combes, 2002):

$$R = (m_w/m_b)4\Theta\omega^2L / 3g, \quad (2)$$

where  $R$  is the ratio of inertial-elastic to aerodynamic bending moments,  $m_w$  is mass of one wing,  $m_b$  is mass of the body,  $\Theta$  is angular stroke amplitude,  $\omega$  is angular frequency,  $L$  is wing span and  $g$  is earth's gravitational acceleration. The ratio of wing to body mass in insects has been shown to vary from 0.5% in bees to 6% in hawkmoths (Ellington, 1984a), and wing span varies widely. However, because the frequency term in the above equation is squared, wing-beat frequency has a large effect on the moment ratio. Thus, many small insects (with higher wing beat frequencies; Dudley, 2000) may actually have higher ratios of inertial-elastic to aerodynamic bending moments, despite having smaller, lighter wings. Our estimates suggest that this ratio is quite large in insects over a broad size range ( $R=7$  in *Manduca* and  $R=6$  in *Drosophila*). Although the magnitude of passive wing bending that actually occurs during flight depends on additional factors (such as the scaling of wing stiffness; Combes and Daniel, 2003a), these results indicate that the spatial and temporal patterns of whatever passive bending does occur are likely to be determined primarily by inertial-elastic effects in many species.

In addition to large variations in size, insect wings display tremendous variability in design features, such as planform wing shape and the arrangement of supporting veins, which could affect how their wings respond to aerodynamic and inertial-elastic forces. Interestingly, despite dramatic visual differences in wing design, overall wing stiffness appears to scale strongly with wing size in a broad range of species

(Combes and Daniel, 2003a). Patterns of regional stiffness variation in insect wings may in fact be affected by wing shape and venation; however, we have measured very similar patterns of stiffness variation in the wings of hawkmoths and aeshnid dragonflies, insects with strikingly different wing designs (Combes and Daniel, 2003b). These results suggest that large differences in insect wing design do not necessarily lead to equivalent differences in wing stiffness and bending behavior.

#### Concluding remarks

Because aeroelastic effects appear to be relatively unimportant in determining dynamic wing shape, an integrative model of insect flight that incorporates passive wing flexibility may be easier to develop than previously thought. Although the experimental work presented in this study addresses the relative contributions of aerodynamic and inertial-elastic forces to wing bending in only one species using a particular kinematic pattern, these results verify recent theoretical studies (Daniel and Combes, 2002) suggesting that fluid-dynamic forces have only a minor effect on passive bending when flexible structures are flapped in air (*versus* water, where fluid forces dominate). In addition, while detailed numerical methods (e.g. Liu et al., 1998; Ramamurti and Sandberg, 2002; Sun and Tang, 2002a; Wang, 2000) will undoubtedly continue to contribute to our understanding of three-dimensional fluid flow around flapping wings, recent work suggests that far simpler analytical methods are able to predict temporal patterns of unsteady force production remarkably well (Sane and Dickinson, 2002). Inserting the dynamic shape of wing sections (as determined by finite element analysis or other inertia-based methods) into quasi-steady models of flight that account for unsteady effects may yield a tractable modeling tool that could be used to explore the effects of wing flexibility on unsteady force production. Models of this type could be used to determine when and how wing flexibility affects aerodynamic force generation, and ultimately contribute to an integrative model of insect flight linking sensory feedback and patterns of muscle force production to dynamic wing motions, force generation and insect flight performance.

The authors would like to thank M. Dillon for his assistance in constructing the vacuum chamber and calibrating the high-speed video cameras, and J. Longnion for his work in salvaging and altering chart recorder motors. E. Goldman provided valuable suggestions regarding data analysis, and M. Tu provided Matlab code for digitizing wing coordinates. K. Flick was instrumental in troubleshooting the high-speed video cameras and J. Dierberger at MSC Software provided crucial assistance with the FEM model. S. Sane, M. Tu and two anonymous reviewers provided helpful comments on drafts of the paper. This work was supported by NSF grant F094801 to T.D., the John D. and Catherine T. MacArthur Foundation, an ONR-MURI grant to T.D., an NSF graduate fellowship to S.C. and an ARCS fellowship to S.C.

#### References

- Batchelor, G. K.** (1967). *An Introduction to Fluid Dynamics*. Cambridge: Cambridge University Press.
- Combes, S. A.** (2002). Wing flexibility and design for animal flight. PhD thesis, University of Washington.
- Combes, S. A. and Daniel, T. L.** (2001). Shape, flapping and flexion: wing and fin design for forward flight. *J. Exp. Biol.* **204**, 2073-2085.
- Combes, S. A. and Daniel, T. L.** (2003a). Flexural stiffness in insect wings: I. Scaling and the influence of wing venation. *J. Exp. Biol.* **206**, 2979-2987.
- Combes, S. A. and Daniel, T. L.** (2003b). Flexural stiffness in insect wings: II. Spatial distribution and dynamic wing bending. *J. Exp. Biol.* **206**, 2989-2997.
- CRC** (2001). *Handbook of Chemistry and Physics*, 81st edition. Cleveland, Ohio: CRC Press.
- Dalton, S.** (1975). *Borne on the Wind: The Extraordinary World of Insects in Flight*. New York: Reader's Digest Press.
- Daniel, T. L.** (1987). Forward flapping flight from flexible fins. *Can J. Zool.* **66**, 630-638.
- Daniel, T. L. and Combes, S. A.** (2002). Flexing wings and fins: bending by inertial or fluid-dynamic forces? *Int. Comp. Biol.* **42**, 1044-1049.
- Dickinson, M. H., Lehman, F.-O. and Sane, S. P.** (1999). Wing rotation and the aerodynamic basis of insect flight. *Science* **284**, 1954-1960.
- Dudley, R.** (2000). *The Biomechanics of Insect Flight: Form, Function, Evolution*. Princeton, NJ: Princeton University Press.
- Ellington, C. P.** (1984a). The aerodynamics of hovering insect flight. Part II: Morphological parameters. *Phil. Trans. R. Soc. Lond. B* **305**, 17-40.
- Ellington, C. P.** (1984b). The aerodynamics of hovering insect flight. Part VI: Lift and power requirements. *Phil. Trans. R. Soc. Lond. B* **305**, 145-181.
- Ennos, A. R.** (1988). The inertial cause of wing rotation in Diptera. *J. Exp. Biol.* **140**, 161-169.
- Ennos, A. R.** (1989). Inertial and aerodynamic torques on the wings of Diptera in flight. *J. Exp. Biol.* **142**, 87-95.
- Lehmann, F.-O. and Dickinson, M. H.** (1997). The changes in power requirements and muscle efficiency during elevated force production in the fruit fly *Drosophila melanogaster*. *J. Exp. Biol.* **200**, 1133-1143.
- Liu, H., Ellington, C. P., Kawachi, K., Van den Berg, C., and Willmott, A. P.** (1998). A computational fluid dynamic study of hawkmoth hovering. *J. Exp. Biol.* **201**, 461-477.
- Liu, H. and Kawachi, K.** (1998). A numerical study of insect flight. *J. Comp. Physics* **146**, 124-156.
- Ramamurti, R. and Sandberg, W. C.** (2002). A three-dimensional study of the aerodynamic mechanisms of insect flight. *J. Exp. Biol.* **205**, 1507-1518.
- Sane, S. P. and Dickinson, M. H.** (2002). The aerodynamic effects of wing rotation and a revised quasi-steady model of flapping flight. *J. Exp. Biol.* **205**, 1087-1096.
- Sun, M. and Tang, J.** (2002a). Unsteady aerodynamic force generation by a model fruit fly wing in flapping motion. *J. Exp. Biol.* **205**, 55-70.
- Sun, M. and Tang, J.** (2002b). Lift and power requirements of hovering flight in *Drosophila virilis*. *J. Exp. Biol.* **205**, 2413-2427.
- Timoshenko, S., Young, D. H. and Weaver, W., Jr** (1974). *Vibration Problems in Engineering*. New York: John Wiley & Sons.
- Wainwright, S. A., Biggs, W. D., Currey, J. D. and Gosline, J. M.** (1982). *Mechanical Design in Organisms*. Princeton: Princeton University Press.
- Wakeling, J. M. and Ellington, C. P.** (1997). Dragonfly flight. III. Lift and power requirements. *J. Exp. Biol.* **200**, 583-600.
- Wang, Z. J.** (2000). Vortex shedding and frequency selection in flapping flight. *J. Fluid Mech.* **410**, 323-341.
- Wilkin, P. J. and Williams, M. H.** (1993). Comparison of the aerodynamic forces on a flying sphingid moth with those predicted by quasi-steady theory. *Physiol. Zool.* **66**, 1015-1044.
- Willmott, A. P. and Ellington, C. P.** (1997). The mechanics of flight in the hawkmoth *Manduca sexta*. I. Kinematics of hovering and forward flight. *J. Exp. Biol.* **200**, 2705-2722.
- Wootton, R. J.** (1990). The mechanical design of insect wings. *Sci. Am.* **November**, 114-120.
- Wu, T. Y.** (1971). Hydromechanics of swimming propulsion. Part 1. Swimming of a two dimensional flexible plate at variable forward speeds in an inviscid fluid. *J. Fluid Mech.* **46**, 337-355.
- Zanker, J. M. and Gotz, K. G.** (1990). The wing beat of *Drosophila melanogaster*. II. Dynamics. *Phil. Trans. R. Soc. Lond. B* **327**, 19-44.